Orthorhombic phase of crystalline polyethylene:
A constant pressure path-integral Monte Carlo study

R. Martoňák,[1,2,*] W. Paul,[1] and K. Binder[1]

[1]*Institut für Physik, KoMa 331, Johannes Gutenberg Universität, Staudingerweg 7, 55099 Mainz, Germany*
[2]*Max-Planck-Institut für Polymerforschung, Ackermannweg 10, 55021 Mainz, Germany*

In this paper we present a path-integral Monte Carlo (PIMC) simulation of the orthorhombic phase of crystalline polyethylene, using an explicit atom force field with unconstrained bond lengths and angles. This work represents a quantum extension of our recent classical simulation [R. Martoňák *et al.*, J. Chem. Phys. **106**, 8918 (1997)]. It is aimed both at exploring the applicability of the PIMC method on such polymer crystal systems, as well as on a detailed assessment of the importance of quantum effects on different quantities. We used the NpT ensemble and simulated the system at zero pressure in the temperature range 25–300 K, using Trotter numbers between 12 and 144. In order to investigate finite-size effects, we used chains of two different lengths, C_{12} and C_{24}, corresponding to the total number of atoms in the supercell being 432 and 864, respectively. We show here the results for structural parameters, like the orthorhombic lattice constants a,b,c, and also fluctuations of internal parameters of the chains, such as bond lengths and bond and torsional angles. We have also determined the internal energy and diagonal elastic constants c_{11}, c_{22}, and c_{33}. We discuss the temperature dependence of the measured quantities and compare to that obtained from the classical simulation. For some quantities, we discuss the way they are related to the torsional angle fluctuation. In the case of the lattice parameters we compare our results to those obtained from other theoretical approaches as well as to some available experimental data. In order to study isotope effects, we simulated also a deuterated polyethylene crystal at low temperature. We also suggest possible ways to extend this study and present some general considerations concerning modeling of polymer crystals. [S1063-651X(98)08102-1]

PACS number(s): 02.70.Lq, 05.30.−d, 07.05.Tp, 61.41.+e

I. INTRODUCTION

Polymer crystals are well known to be intrinsically difficult to prepare in a highly crystalline state, which in turn hinders the possibilities of their experimental characterization. As a consequence, computer simulation appears to be a convenient tool to study their properties. For crystalline polyethylene (PE), which represents the simplest and thus paradigmatic case, it has been recently shown [1] that classical constant pressure Monte Carlo (MC) simulation is a well applicable simulation method, provided a good quality force field is available. It allows one to calculate the whole variety of static local and collective quantities, including properties of major practical and technological importance, like thermal expansion and elastic constants. On the other hand, recent work on the same system, using a quasiharmonic or self-consistent quasiharmonic approximation [2–4], has clearly pointed to a quantitative as well as a qualitative inadequacy of the classical treatment at low temperatures, where quantum effects cannot be neglected anymore.

Generally, quantum effects are known to be important in lattice dynamics of solids in the low-temperature region, when classical thermal fluctuations become comparable to or smaller than the amplitude of the quantum zero-point motion. Under particular circumstances, when two different

crystal structures have classically very close energies, and the system is close to a structural phase transition, quantum fluctuations can play a decisive role. In the case of solid nitrogen [5], they are responsible for a strong isotope effect on the low-temperature α-γ structural phase transition as a function of pressure. If the classical energy difference is small enough, quantum effects can even suppress the transition altogether, and stabilize the disordered phase, as it happens in the case of quantum paraelectrics $SrTiO_3$ or $KTaO_3$, where the ferroelectric long-range order is only incipient down to $T=0$ [6]. Even though a PE crystal does not represent such a dramatic case, at low temperatures it is not possible to account even qualitatively for the temperature dependence of quantities like thermal expansion coefficients and elastic constants without quantum effects being duly taken into account.

A natural extension of the classical MC method in order to include quantum effects at finite temperature is the path-integral Monte Carlo (PIMC) scheme [7]. Recently, the NpT version of this method has been applied to study quantum effects in crystals at low temperatures, in particular in solid rare gas systems [8], and silicon crystal [9]. In the case of polymer crystals, the distinguishing feature is an extreme anisotropy, closely related to the existence of many energy scales, ranging from soft intermolecular (nonbonded) interactions to stiff intramolecular (bonded) interactions. This feature presents a problem already at the classical level, as discussed in [10,11,1], and requires an introduction of special global moves in the sampling algorithm. In the quantum case, we should moreover expect very different convergence properties of different physical quantities as a function of Trotter number, depending on the typical energy scale with

―――――
*Permanent address: Department of Physics, Faculty of Electrical Engineering, Slovak Technical University, Ilkovičova 3, 812 19 Bratislava, Slovakia.

which a given quantity is associated.

The aim of this paper is basically twofold. On the one hand, we explore the applicability of the constant pressure PIMC method to a PE crystal, and determine the region of temperatures where the use of the method is practical. On the other hand, since the PIMC scheme is capable of providing essentially exact results, it can also be used to assess the range of validity of approximate analytical methods, like, e.g., quantum quasiharmonic approximation [2–4]. This is particularly important for the study of intrinsically anharmonic phenomena, like, e.g., lattice thermal expansion.

The paper is organized as follows. In Sec. II, we briefly describe the PIMC simulation method used, without addressing the force field and its implementation, since these issues have already been discussed in detail in [1]. In Sec. III, we present and discuss the results, paying particular attention to a comparison of the quantum results to the classical ones. In the final Sec. IV we draw some conclusions and suggest some possible ways to extend this study. We also make several remarks concerning general issues related to modeling of polymer crystals. For completeness, in Appendix A we present the full form of the force field we have used together with numerical values of the parameters. In Appendix B, we present some considerations on the relation of correlation functions of torsional fluctuations to the contraction of the crystal along the chain axis.

II. PIMC SIMULATION METHOD

In this section, we will describe only those features of the simulation method that are specific for the constant pressure PIMC scheme. The implementation of the Sorensen-Liau-Kesner-Boyd (SLKB) force field [12] we used as well as many other features of the present algorithm are exactly identical to those of our classical simulation, which has been described in detail in Ref. [1]. For convenience, however, in Appendix A we summarize the form and parameters of the force field.

We have implemented the constant pressure PIMC scheme basically along the same lines as it was done for a cubic system in Ref. [8], the only difference being that in our case we had to use an anisotropic version of the NpT ensemble. We have used the primitive decomposition of the Hamiltonian, resulting in the effective Hamiltonian

$$H_P(\{\vec{r}_i^k\}) = \sum_{k=1}^{P} \left(\sum_{i=1}^{N} \frac{m_i P}{2\hbar^2\beta^2}(\vec{r}_i^k - \vec{r}_i^{k-1})^2 + \frac{1}{P}V(\{\vec{r}_i^k\}) \right),$$

(1)

where N is the number of particles in the quantum system, m_i are their masses, P is the Trotter number, $\beta = 1/k_B T$ is the inverse temperature, and $V(\{\vec{r}_i\})$ is the potential energy of the system. Such an effective Hamiltonian represents a pseudoclassical system consisting of P copies (Trotter slices) of the original system, individual particles in neighboring Trotter slices being connected via harmonic ''springs,'' and periodic boundary conditions being applied along the Trotter direction. This pseudoclassical system has now NP particles and can be simulated using the same constant pressure MC algorithm as in the classical case. The acceptance criterion for the volume moves was based on the Boltzmann factor

$(s_1 s_2 s_3)^{NP} e^{-\beta E_P}$, where $E_P = H_P + pV_0 s_1 s_2 s_3$, p is the external pressure, V_0 is the volume of the reference supercell, and s_1, s_2, s_3 are three independent scaling factors along the coordinate axes. In all simulations described in this paper, the external pressure was set to zero. The estimators for all configurational properties, diagonal in the coordinate representation, are straightforward analogs of their classical counterparts, while for the kinetic energy we used the virial estimator [13].

To sample the system, we have used three kinds of moves: classical moves, quantum moves, and volume moves. Classical moves of two types, local moves of atoms or global moves of whole polymer chains, as described in Refs. [10,11,1], have always been applied to all particles or chains with a given number in all Trotter slices simultaneously. These moves sample the classical configurational phase space of the system. We note here that when performing a rotation of a given chain in all Trotter slices, the energies of the ''harmonic springs'' between the corresponding individual particles have to be recalculated explicitly, in contrast to pure translational moves of a particle in all Trotter slices, which preserve the energy of the ''springs.'' Quantum moves consisted of local translational moves of individual particles of the pseudoclassical system, which sample the quantum fluctuations around the classical paths. In the quantum moves, different maximum displacements have been used for C and H atoms, not only because of the different number of bonds but also because of the different mass of the atoms and resulting different stiffness of the ''springs.'' In volume moves, we performed a simultaneous rescaling of coordinates of all particles in all Trotter slices by the three scaling factors s_1, s_2, s_3. One Monte Carlo step per site (MCS) thus consisted of an attempted quantum move on each particle of the pseudoclassical system, followed by a classical move attempted successively on all atoms or all chains (always simultaneously in all Trotter slices, as described above) and a volume move. Among the classical moves, 30% of global moves were used, as in the classical study [1]. For all kinds of moves, the displacements were chosen to yield an acceptance ratio of 20–30%.

We have simulated systems with C_{12} and C_{24} chains, consisting of $2\times3\times6$ and $2\times3\times12$ unit cells, respectively (432 and 864 atoms), at temperatures 25, 50, 100, 150, 200, and 300 K. At different temperatures, different numbers of values of the Trotter number were used. For the smaller system, we used at 25 K $P=144$, at 50 K $P=54,72,144$, at 100 K $P=36,54,72$, at 150 K $P=48$, at 200 K $P=16,24,32$, and finally at 300 K $P=12,16,24$. The larger system was simulated only at 100 K with $P=72$ and at 300 K with $P=24$. We note here that the largest pseudoclassical systems simulated consisted of $432\times144 = 864\times72 = 62208$ particles, which is quite a large number. As an initial configuration for a given temperature, we always used a pseudoclassical system consisting of P identical copies of an equilibrated classical configuration at the same temperature. This configuration was then equilibrated for several thousand MCS with the full PIMC algorithm, which corresponded to switching on the quantum fluctuations and allowing the system to find a new equilibrium. For illustration of the run length used for measurement, for the smaller system at 300 K and $P=24$ we used about 280 000 MCS. Roughly the same amount of CPU

time was used for all data points, the number of Monte Carlo steps per site thus scaling inversely with the number of particles NP of the pseudoclassical system. The whole run consisted of numbers of subbatches ranging from 5 to 57 and the batch subaverages were used to estimate the approximate error bars of the total averages.

III. RESULTS AND DISCUSSION

Before discussing in detail the results for various quantities, we comment briefly on convergence of the PIMC scheme as a function of the Trotter number P. For different quantities, we have found considerably different convergence, the best case being that of quantities like, e.g., lattice constants, which are mainly related to softer interactions (nonbonded interactions and torsional terms). In such cases, where the results obtained with different values of Trotter number P were identical within the statistical error, the quantum limit was practically reached and no extrapolation was necessary. A considerably slower convergence is found for quantities such as the energy, which depend crucially on fluctuations of degrees of freedom related to strong (bonded) interaction potentials. In these cases, an extrapolation to $P \rightarrow \infty$ was performed in order to recover the true quantum values. We have used the standard formula [14]

$$A_P = A_\infty + \frac{a}{P^2} + \frac{b}{P^4} + O\left(\frac{1}{P^6}\right), \qquad (2)$$

which requires data for three different values of Trotter number P in order to find the extrapolated value A_∞.

In the discussion, we concentrate mainly on the comparison of quantities obtained from the quantum simulation to their classical counterparts, presented in [1]. We start with the local quantities, in particular fluctuations of the internal coordinates, for which the quantum effects are found to be most pronounced.

In Figs. 1 and 2, we show the temperature dependence of the average bond length fluctuation for C-C and C-H bonds, respectively. The distinguishing feature of quantum results for such fluctuations is their saturation at rather large values at low temperatures, instead of the classical vanishing $[\sqrt{\langle (\delta r)^2 \rangle} \propto \sqrt{T}$ as $T \rightarrow 0$ in the classical case]. In particular in the case of the C-H bond, there is a marked Trotter dependence of the results. By means of the above described extrapolation, we found at $T = 50$ K the values of 0.05 Å for $\sqrt{\langle (\delta r_{CC})^2 \rangle}$ and 0.079 Å for $\sqrt{\langle (\delta r_{CH})^2 \rangle}$, which represent about 3% and 7% of the respective equilibrium bond length. These values are representative of the ground state values, since both curves appear to be entirely flat up to room temperature, reflecting high frequencies of corresponding bond stretching phonon modes. In Figs. 3 and 4, average fluctuations of the bond angles θ_{CCC} and θ_{HCH} are shown as a function of temperature. Trotter extrapolation at $T = 50$ K yields here the values of 3.46° and 8.44° for $\sqrt{\langle (\delta \theta_{CCC})^2 \rangle}$ and $\sqrt{\langle (\delta \theta_{HCH})^2 \rangle}$, respectively. While the former curve increases at room temperature by about 0.5° with respect to the ground state value, the latter one corresponding to the bond angle involving two hydrogen atoms is completely flat.

In Fig. 5, we show the temperature dependence of the average torsional angle fluctuation $\sqrt{\langle \phi_{CCCC}^2 \rangle}$ from the trans
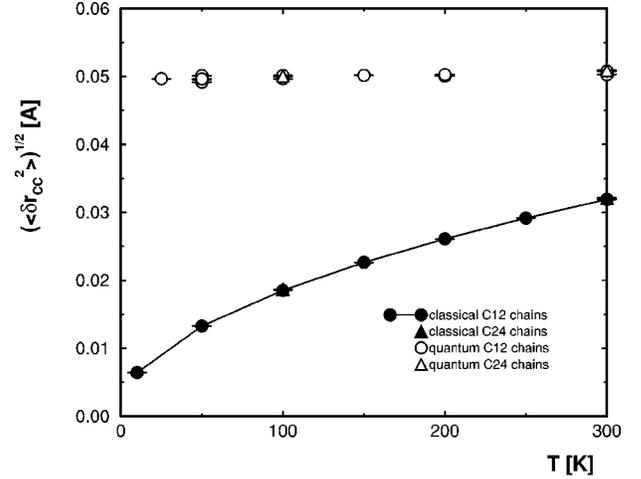
FIG. 1. Temperature dependence of the average fluctuation $\sqrt{\langle (\delta r_{CC})^2 \rangle}$ of the C-C bond length, in the classical and the quantum case, shown for different system sizes. In this and most of the following figures, statistical error bars are shown; lines are for visual help only. In all figures, the same symbol is used for quantum results corresponding to different values of the Trotter number P. When at a given temperature the results for different values of P are indistinguishable within the statistical error, as in this figure, the Trotter numbers are not indicated explicitly.

minimum, which already in the classical case [1] has been shown to play an important role in the physics of the system. The values at $T = 50$ K and $T = 25$ K are already very close to each other, and therefore the $T = 25$ K value of 5.59° can be considered to be representative of the ground state. The characteristic temperature, below which the difference between the classical and quantum values starts to increase rapidly, can be estimated to be about 150 K. At room temperature, the difference is still about 0.5°.

The internal energy per unit cell of the system is shown in Fig. 6. The dependence on P is in this case particularly pro-
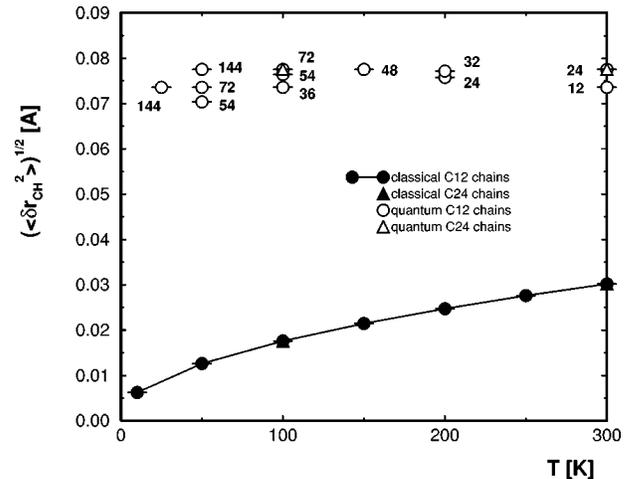
FIG. 2. Temperature dependence of the average fluctuation $\sqrt{\langle (\delta r_{CH})^2 \rangle}$ of the C-H bond length, in the classical and the quantum case, shown for different system sizes. When the quantum results at a given temperature exhibit a pronounced dependence on the Trotter number P, as in this figure, the corresponding values of P are indicated next to the symbols.
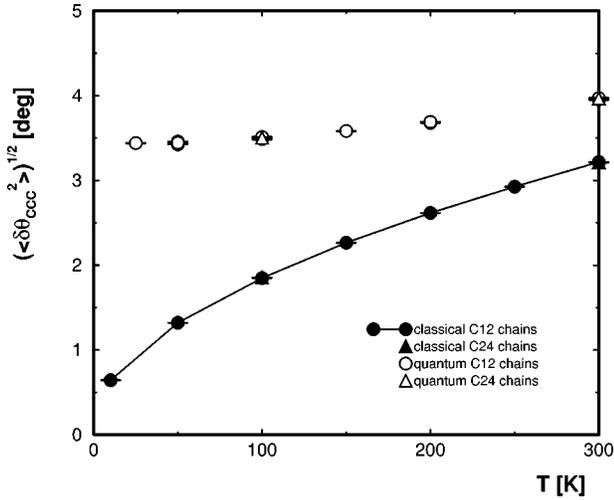
FIG. 3. Temperature dependence of the average fluctuation $\sqrt{\langle(\delta\theta_{CCC})^2\rangle}$ of the C-C-C bond angle, in the classical and the quantum case, shown for different system sizes.

nounced, since the dominant contribution at low temperatures comes from the hard degrees of freedom that require larger values of the Trotter number in order to converge. The extrapolation to $P\rightarrow\infty$ is thus absolutely necessary here, and has been performed for all temperatures where data for three values of P are available, i.e., 50, 100, 200, and 300 K. The extrapolated values at 50 and 100 K suggest that the energy in this region would still somewhat decrease by approaching zero temperature and the extrapolated value of 62.125 kcal/mol at 50 K can be considered as an upper estimate of the ground state total energy. By subtracting the classical ground state energy, which is found to be equal to -7.39 kcal/mol per unit cell, we find a value of 17.38 kcal/mol per CH_2 group, which agrees well with the zero-point energy of 17.598 kcal/mol, obtained in Ref. [15] within quasiharmonic approximation for a different force field.

Concerning the structural stability, for the smaller system we observed at $T=300$ K an occasional rotation of a whole
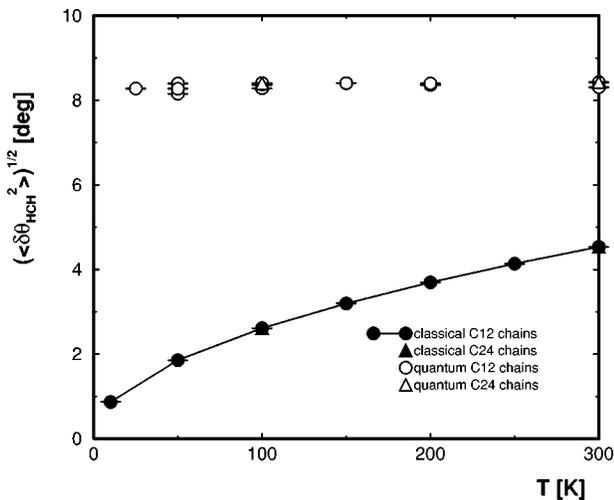
FIG. 4. Temperature dependence of the average fluctuation $\sqrt{\langle(\delta\theta_{HCH})^2\rangle}$ of the H-C-H bond angle, in the classical and the quantum case, shown for different system sizes.
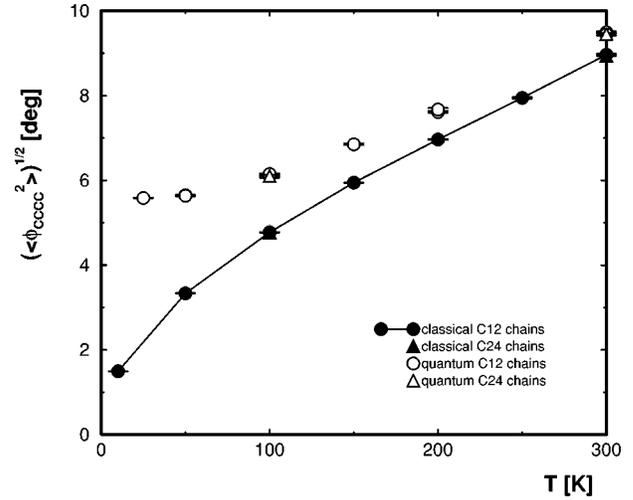
FIG. 5. Temperature dependence of the average torsional angle fluctuation $\sqrt{\langle\phi^2_{CCCC}\rangle}$ from the trans minimum, in the classical and the quantum case, shown for different system sizes.

chain from the "herringbone" structure, just as in the classical case [1]. No such rotation was observed for the larger system, however.

Before passing to the discussion of the temperature dependence of the lattice constants a, b, and c, we would like to make a general comment on the statistical error of lattice constants of crystals evaluated within constant pressure PIMC scheme. The statistical error $\sigma(\langle a\rangle_{run})$ of the lattice constant $\langle a\rangle_{run}$ averaged over a run consisting of N configurations is given by

$$\sigma(\langle a\rangle_{run})=\frac{\sigma(a)}{\sqrt{N/s}}, \qquad (3)$$

where $\sigma(a)$ is the intrinsic fluctuation of the quantity a, and s is the corresponding statistical inefficiency, expressing the effect of correlations between subsequent configurations of
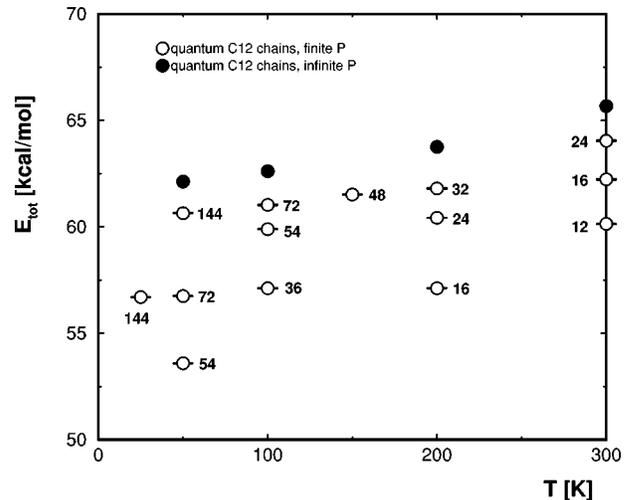
FIG. 6. Temperature dependence of the internal energy per unit cell of a quantum system with C_{12} chains, shown for different values of the Trotter number P, together with an extrapolation to $P\rightarrow\infty$. Note the strong dependence on the Trotter number P.
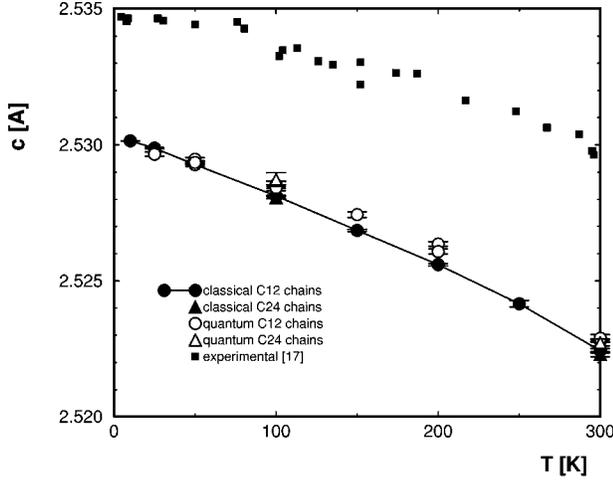
FIG. 7. Temperature dependence of the lattice parameter c, in the classical and the quantum case, shown for different system sizes, together with the experimental data [17].

the Monte Carlo run [16]. In order to keep the Trotter error roughly constant at different temperatures, one usually keeps the product PT constant. For given system size and amount of CPU time, the number of configurations N is inversely proportional to the Trotter number P and thus directly proportional to temperature T. On the other hand, the fluctuation $\sigma(a)$ of the lattice constant a is essentially a fluctuation of the linear size of the system, which is a purely classical fluctuation, and obeys the equipartition theorem. Provided the elastic constants of the system do not vary too much, which should be well satisfied at low temperatures, the relation $\sigma^2(a) \sim T$ should hold. Combining the expressions together, we find

$$\sigma(\langle a \rangle_{\text{run}}) \sim \frac{\sqrt{T}}{\sqrt{T/s}} \sim \sqrt{s}, \qquad (4)$$

where the explicit dependence on T in the numerator and denominator has canceled. Of course, there is still an implicit dependence hidden in the factor s, which increases with decreasing temperature because of growing system size in the Trotter direction. Nevertheless, in the case of such a purely classical fluctuation which vanishes as $T \to 0$, the situation is more favorable with respect to the case of a general fluctuation, which would instead tend to a finite zero-point quantum value. In our results for the lattice constants, this is illustrated by the fact that the error bars of points at lowest temperatures are not larger than those of points at higher temperatures.

The temperature dependence of the lattice constant c is shown in Fig. 7. In both classical and quantum cases a lattice contraction with increasing temperature is observed. An interesting feature here is that at $T \sim 50$ K, the classical and quantum curves cross. At higher temperatures, the quantum result stays above the classical one while falling slightly below that for $T < 50$ K, where the quantum flattening appears. This behavior suggests the presence of at least two distinct quantum effects. Since in the classical case [1] it turned out that there is a linear dependence between c and $\langle \phi^2_{\text{CCCC}} \rangle$, we have tried the same plot for our quantum data, Fig. 8, in
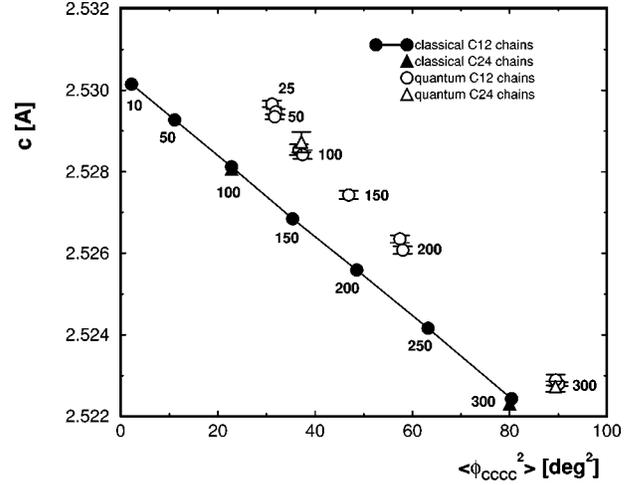
FIG. 8. Lattice parameter c vs $\langle \phi^2_{CCCC} \rangle$, in the classical and the quantum case, shown for different system sizes. Note that also in the quantum case, the dependence is almost linear over the whole temperature range. The values of temperature, which is a parameter of the plot, are indicated next to the symbols.

order to separate different contributions. In the latter plot, the classical and quantum curves are roughly parallel to each other, which shows that the low-temperature flattening of c is a consequence of freezing of the thermal contribution to the torsional fluctuations. With the exception of the lowest temperatures, the shift of the quantum curve with respect to the classical one appears to be temperature independent, being roughly equal to 0.0015 Å. This represents a zero-point expansion of the lattice along the c direction arising from hard modes that are not significantly excited even at room temperature. While in the classical case all points are found to fall very well on a straight line in the whole temperature range [1], in the quantum case a distinct upward bending of the curve is apparent at low temperatures. To understand its origin, one might try to use the full formula

$$c = c_0 \left(1 - \frac{1}{4}\sin^2\frac{\alpha}{2} \frac{1}{2}\langle (\phi_0 - \phi_1)^2 \rangle \right)$$
$$= c_0 \left[1 - \frac{1}{4}\sin^2\frac{\alpha}{2} \langle \phi_0^2 \rangle \left(1 - \frac{\langle \phi_0 \phi_1 \rangle}{\langle \phi_0^2 \rangle} \right) \right], \qquad (5)$$

derived in Ref. [3] (see also Appendix B), which relates the contraction of the lattice constant c to correlation functions of two neighboring torsional angle fluctuations ϕ_0, ϕ_1. The temperature dependence of the normalized correlation function $\langle \phi_0 \phi_1 \rangle / \langle \phi_0^2 \rangle$ is shown in Fig. 9. In contrast to the classical curve, which is flat in the whole temperature region, the quantum one is seen to increase in value at low temperatures where it becomes almost a factor of two larger than the classical one. In Fig. 10 we plot c versus $\frac{1}{2}\langle (\phi_0 - \phi_1)^2 \rangle$. In this plot, the low temperature upward bending from Fig. 8 has become less pronounced and the points now exhibit a clear linear dependence, which suggests that the bending has its origin in the quantum reinforcement of the correlation function $\langle \phi_0 \phi_1 \rangle / \langle \phi_0^2 \rangle$ of neighboring torsions at low temperatures. The slope of 1.275×10^{-4} Å deg^{-2}, however, turns out to be larger in magnitude by a factor of two with respect to
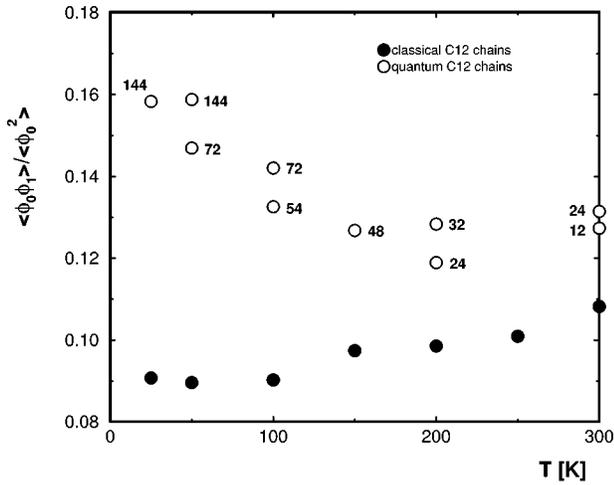
FIG. 9. Temperature dependence of the normalized correlation function $\langle \phi_0 \phi_1 \rangle / \langle \phi_0^2 \rangle$ of fluctuations of two neighboring torsional angles from the trans minima, in the classical and the quantum case, for the system with C_{12} chains. Note the pronounced dependence on the Trotter number P.

the value of $\frac{1}{4} c_0 \sin^2(\alpha/2)(\pi/180)^2 = 6.22 \times 10^{-5}$ Å deg^{-2} resulting from Eq. (5) (we took the values $c = 2.53$ Å and $\alpha = 180° - 110.75°$). About the same discrepancy in the slope is found also for the classical data, and this has been pointed out already in Ref. [1] (where, however, the correlation function between neighboring torsions was neglected and the discrepancy thus turned out to be just about a factor of 1.5). While in the classical case the thermal contraction could be modified due to contribution of modes other than torsions, in the quantum case such harder modes are mostly frozen even at room temperature, and do not contribute considerably. Thus in the quantum case the formula (5) should yield a better agreement with the simulation. As it turns out, however, it captures qualitatively correctly the basic role of torsional correlation functions in the thermal contraction, but
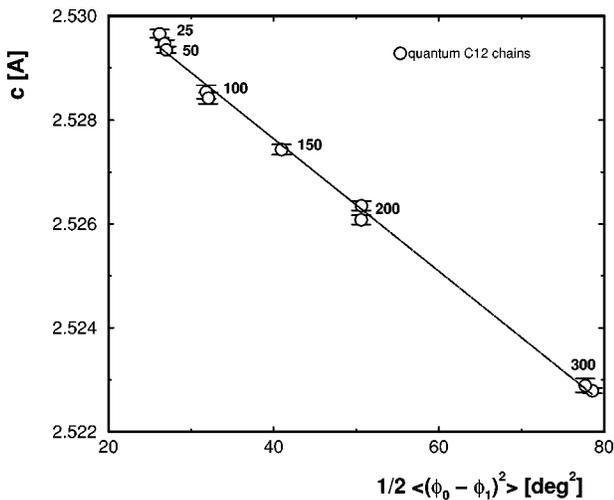
FIG. 10. Lattice parameter c vs $\frac{1}{2}\langle(\phi_0 - \phi_1)^2\rangle$ in the quantum case for system with C_{12} chains. The values of temperature, which is a parameter of the plot, are indicated next to the symbols. The points can be fitted by a line $c = 2.5327 - 1.275 \times 10^{-4} \frac{1}{2}\langle(\phi_0 - \phi_1)^2\rangle$.
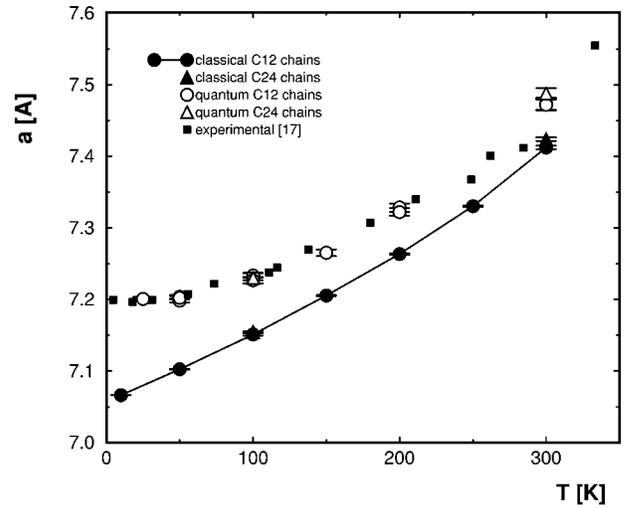
FIG. 11. Temperature dependence of the lattice parameter a, in the classical and the quantum case, shown for different system sizes, together with the experimental data [17].

fails in the quantitative aspect. We discuss the origin of this discrepancy in detail in Appendix B. Analogously to the classical case, no significant finite-size effects are seen on the lattice constant c. Comparing the quantum result to experimental data [17] in Fig. 7, we see that apart from the constant offset, the agreement has improved at low temperatures, due to the quantum flattening.

In Fig. 11, we show the temperature dependence of the lattice constant a. At temperatures below 50 K, the quantum curve appears to be entirely flat, and the difference between the quantum and the classical result is in this region as large as 0.13 Å, which represents a 2% effect. At all temperatures, the quantum curve lies above the classical one. It is interesting to note that the difference between the two curves persists up to room temperature, being at $T = 300$ K equal to 0.06 Å, which is still about a half of the zero-temperature value. For this lattice constant, a very good agreement between the simulation and experimental results [17] is found, which proves that almost the whole low-temperature discrepancy between the classical simulation results and experiment is purely due to quantum effects. Similarly to the classical case, no finite-size effect is seen on the quantum curve at $T = 100$ K, while a small one is seen at $T = 300$ K.

Analogously to the case of the lattice constant c, in Fig. 12 we plot the lattice constant a versus $\langle \phi_{CCCC}^2 \rangle$. Interestingly, in such a ''scaling'' plot, both classical and quantum results are found to collapse nearly on the same straight line, which shows that the lattice constant a does not depend on temperature explicitly, but only implicitly, through the temperature dependence of the torsional fluctuations. Since the latter dependence is very different in the classical and quantum cases, the behavior of a is also substantially different.

In Fig. 13, the temperature dependence of the lattice constant b is shown. Similarly to the classical case, the error bars for b are larger than those for a. The quantum flattening at low temperatures is now less pronounced, and in order to find the limiting zero-temperature value of b, it would be necessary to go to even lower temperatures than 25 K. Here again, the quantum curve lies above the classical one at all temperatures. At 25 K, the difference between them is about
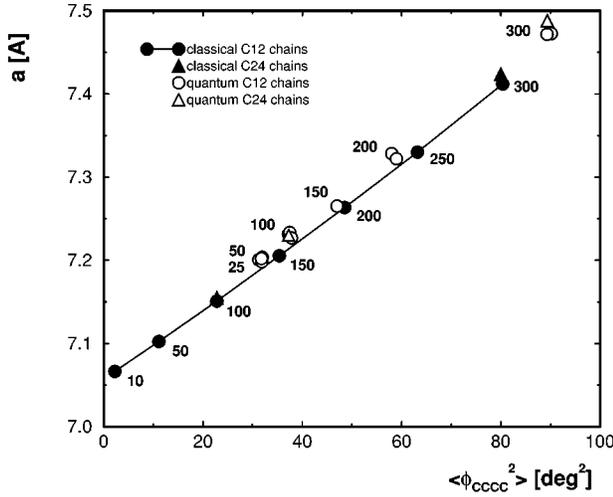
FIG. 12. Lattice parameter a vs $\langle \phi_{CCCC}^2 \rangle$, in the classical and quantum case, shown for different system sizes. The values of temperature, which is a parameter of the plot, are indicated next to the symbols. Note the collapse of both classical and quantum results on almost the same straight line over the whole temperature range.

0.03 Å, which represents a 0.6% effect, while at 300 K it decreases to about 0.02 Å. A finite-size effect very similar to the one in the classical case is observed here too. It is visible already at 100 K, where the point for the system with C_{24} chains falls slightly below that for the system with C_{12} chains, while being strongly pronounced at 300 K, where the difference is about 0.035 Å. The same finite-size effect is also visible in the ''scaling'' plot in Fig. 14, where moreover at lower temperatures a downward bending of the quantum curve can be observed. Comparison to the experimental data [17] in Fig. 13 in this case appears to be less good than in the case of a, however, for a detailed comparison simulation data for larger system sizes would be required.

We have also computed the diagonal elastic constants c_{11}, c_{22}, c_{33} of the system. Analogously to the classical case [1], we evaluated c_{11}, c_{22} from the Parrinello-Rahman fluctuation formula [18],
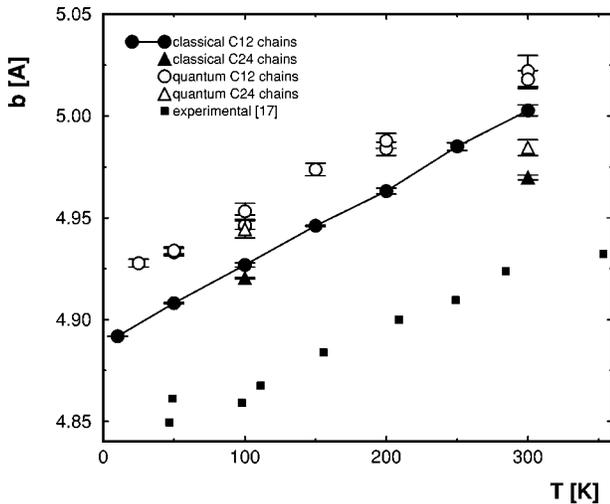
FIG. 13. Temperature dependence of the lattice parameter b, in classical and quantum case, shown for different system sizes, together with the experimental data [17]. Note the strong finite-size effect at higher temperatures for both classical and quantum results.
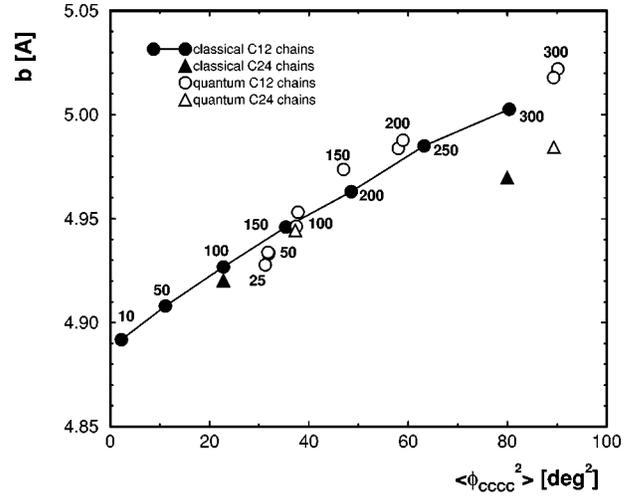
FIG. 14. Lattice parameter b vs $\langle \phi_{CCCC}^2 \rangle$, in the classical and the quantum case, shown for different system sizes. The values of temperature, which is a parameter of the plot, are indicated next to the symbols. Note the strong finite-size effect at higher temperatures for both sets of data as well as the downward bending of the quantum curve at low temperatures.

$$c_{ik} = \frac{k_B T}{\langle V \rangle} \langle e_i e_k \rangle^{-1}, \quad i,k = 1,2,3, \quad (6)$$

while for c_{33} we used the Gusev-Zehnder-Suter formula [19] in its approximate version suitable for small strain fluctuations

$$c_{ik} = -\sum_n \langle p_i e_n \rangle \langle e_n e_k \rangle^{-1}, \quad (7)$$

where V is the supercell volume and p_i and e_i are the diagonal components of the pressure tensor and strain tensor, respectively. This choice of methods was motivated by the finding that in the classical case [1] significantly smaller statistical errors resulted for c_{33} from the Gusev-Zehnder-Suter formula (7), while for the other elastic constants errors were slightly smaller for the Parrinello-Rahman fluctuation formula (6). Both formulas are classical and their use for evaluation of elastic constants also in case of PIMC technique is justified by the fact that strain fluctuations are classical objects that have the same values in all Trotter slices. The results are shown on Figs. 15, 16, and 17. The data for c_{11} exhibit a flattening at low temperatures and suggest that the ground state value is reduced with respect to the classical one by about 2 GPa. A similar conclusion might be true also for c_{22}, where the large statistical error precludes a more detailed comparison. The best results are obtained for c_{33}, analogously to the classical case. Here the flattening is clearly seen and the ground state value is reduced due to quantum effects by about 20 GPa. In Fig. 18, c_{33} is plotted against $\langle \phi_{CCCC}^2 \rangle$. The quantum points fall close to the line of collapse of the classical points, which indicates that a dominant part of the quantum softening of c_{33} has its origin in the finite value of zero-point torsional fluctuations. Not surprisingly, error bars of the quantum data are much larger compared to the corresponding classical ones. Our results show that for a strongly anisotropic crystal, in might be possible to
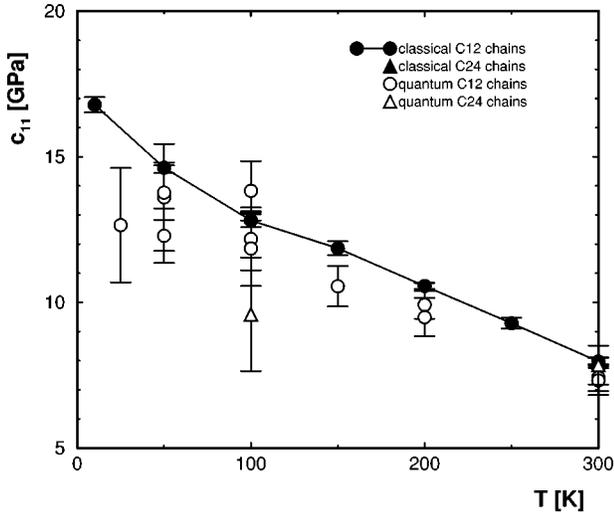
FIG. 15. Elastic constant c_{11} as a function of temperature, in both the classical and the quantum case, shown for different system sizes.

obtain fairly good results for some components of the tensor of elastic constants, while other components might be much more difficult to compute. In any case, calculation of elastic constants within the PIMC scheme is at present computationally very demanding.

Finally, we have also studied isotope effects by simulating deuterated PE. In this case, we have performed the simulation only at the lowest temperature $T = 25$ K, with the same system size and Trotter number as in case of normal (hydrogenated) polyethylene. The results for some quantities are summarized in Table I. All three lattice constants are shorter in deuterated PE. The largest effect is seen on the lattice constant a, while in case of b its relative magnitude is smaller by a factor of 3 and in that of c by a factor of 20.

IV. CONCLUSIONS

In this paper, we have demonstrated that for system sizes of several hundred atoms, PIMC is a practical method allow-
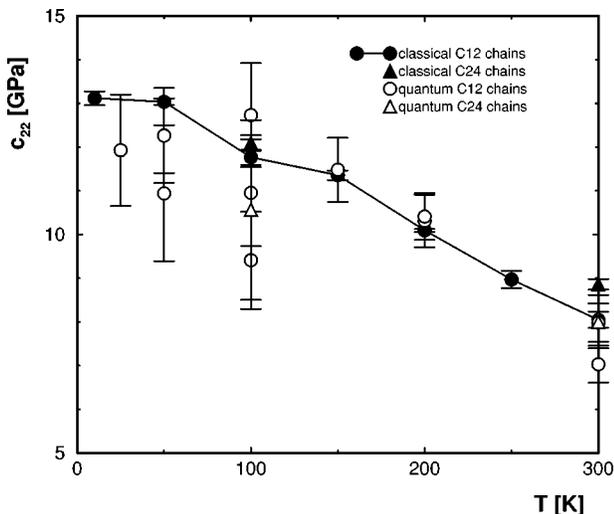
FIG. 16. Elastic constant c_{22} as a function of temperature, in both the classical and the quantum case, shown for different system sizes.
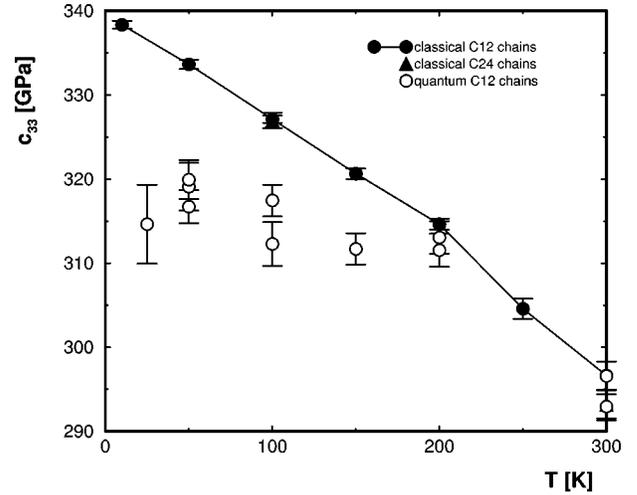
FIG. 17. Elastic constant c_{33} as a function of temperature, in both the classical and the quantum case, shown for different system sizes.

ing a fully quantum simulation of crystalline systems with many different energy scales, like realistic explicit atom models for polymer crystals with no constraints on the degrees of freedom. Even in the low-temperature region, where the system is close to its ground state, it is possible to calculate lattice constants and internal coordinates with a fairly good accuracy. On the other hand, an accurate determination of elastic constants is still very difficult. The limitations of the method in a study of the thermal expansion of the PE crystal are mainly set by the fact that the finite-size effects in the quantum case are more pronounced with respect to the classical one, while at the same time it is more difficult to simulate larger systems, because of the extra Trotter dimension. It would be very helpful to have for an anisotropic crystal a combined finite-size scaling scheme, allowing a simultaneous extrapolation of lattice constants to thermodynamic limit and Trotter limit, analogous to the one developed
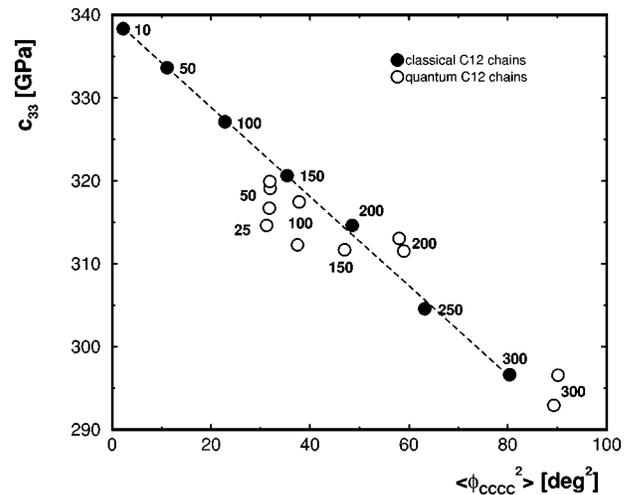
FIG. 18. Elastic constant c_{33} vs $\langle \phi^2_{\text{CCCC}} \rangle$, in both the classical and the quantum case, for system with C_{12} chains. The values of temperature, which is a parameter of the plot, are indicated next to the symbols. Note that the quantum results fall close to the line passing through the classical results.

TABLE I. Isotope effect: deuterated PE compared to normal (hydrogenated) PE. All values correspond to the system with C_{12} chains and $P = 144$ at $T = 25$ K. No extrapolation to $P \to \infty$ has been performed here.

	Normal PE	Deuterated PE	Difference
a	7.201 ± 0.003 Å	7.170 ± 0.003 Å	-0.43%
b	4.928 ± 0.002 Å	4.921 ± 0.002 Å	-0.14%
c	2.5297 ± 0.0001 Å	2.5292 ± 0.0001 Å	-0.02%
$\sqrt{\langle \phi_{CCCC}^2 \rangle}$	$5.59 \pm 0.01°$	$5.26 \pm 0.015°$	-5.9%
$\sqrt{\langle (\delta \theta_{HCH})^2 \rangle}$	$8.28 \pm 0.001°$	$7.17 \pm 0.003°$	-13.4%
$\sqrt{\langle (\delta r_{CH})^2 \rangle}$	0.074 ± 0.00001 Å	0.065 ± 0.00001 Å	-12.1%

in Ref. [8] for the specific heat of a cubic crystal. A prerequisite for such scaling, however, is an availability of high-accuracy data. A possible route here might be an improvement on the primitive PIMC algorithm by using a better approximation to the density matrix, similar to that used for liquid ^{4}He in Ref. [7], allowing a substantial reduction of the Trotter number. In a polymer crystal, the stiffest parts of the potential are the bond stretching terms, which formally have a form of pair interactions between neighboring atoms. For such pair interactions, it is possible to calculate the exact two-body density matrix, either by means of expansion in eigenfunctions, or by matrix squaring. This exact form could be tabulated and used in the simulation, while the rest of the potential would be treated in a standard way. Such a trick can be expected to considerably improve the Trotter convergence, which in turn would enable simulation of larger systems and increase the statistical accuracy of the results.

A detailed comparison to a quasiharmonic approximation will be done in a forthcoming paper [20]. It would also be of interest to perform such an approximation for finite lattices in order to clarify the physical origin of the finite-size effects in both classical and quantum cases, which still remain to be understood.

Concerning the physics of the system, we have demonstrated that in both the classical and the quantum case, the torsional fluctuations play a central role in the thermal expansion of the system. It would be desirable to have an analytical theory of the lateral thermal and zero-point expansion, allowing one to understand the origin of the anisotropy in both cases. We have determined also some local quantities, in particular zero-point fluctuations of internal coordinates, like bond lengths and bond and torsional angles, knowledge of which might be of relevance for local experimental techniques.

Finally, we would like to make a few remarks concerning modeling of polymer crystals in general, taking into account quantum effects. It seems to us that for this sort of system, force field building lags somewhat behind the development of simulation methods, concerning in particular the ability to reproduce anharmonic effects correctly. As already pointed out in Ref. [1], in the classical limit, where in principle all phonon modes can contribute to the thermal expansion of the system, there is a substantial difference between the properties of SLKB force field [12] and Karasawa-Dasgupta-Goddard (KDG) force field [15], as far as the thermal expansion coefficient α_3 is concerned. In the case of the former one, α_3 is classically negative at all temperatures, and originates dominantly from torsional fluctuations, while for the latter one it vanishes as $T \to 0$ [2], which points to a large

contribution of other modes. Such behavior might perhaps have to do with the equilibrium values in the bond stretching and angle bending terms since for the KDG force field these are substantially different from their average values, which in our opinion does not seem to be sufficiently justified. This also demonstrates that the properties of a polymer crystal are much more sensitive to the details of the force field than those of a liquid. In order to have a systematic control of the important anharmonic properties of a solid polymer system, an improvement on the side of the force field building is necessary. Such improvement would allow one to explore fully the potential of existing classical and quantum simulation methods. One first and relatively simple thing to do in order to develop force fields suitable for quantum simulations would be to use a quantum quasiharmonic approximation to determine the ground state structure, instead of bare energy minimization, for fitting force fields to experimental structures. Obviously, a prerequisite for this is a better experimental characterization of the system in the whole range of temperatures, making use of up-to-date experimental techniques, such as, e.g., x-ray diffraction with synchrotron sources. Such techniques should also allow a precise experimental determination of isotope effects on lattice constants and thermal expansion, which might in principle help one to decide which of the above-mentioned force fields provides a better description of the real PE crystal. While for the SLKB force field the difference between classical and quantum value (the isotope effect is also related to this difference) of α_3 tends to vanish in the temperature region over 200 K, where the torsional fluctuations become thermally activated, in case of the KDG force field a large difference persists up to room temperature [2]. Accurate measurements of all components of the tensor of elastic constants in a wide region of temperatures would also be very interesting and helpful.

APPENDIX A

In this Appendix, we present the full form of the force field used in our present quantum and previous classical simulation [1], which is a slightly modified version of the SLKB force field [12]. While the formal modifications have been described in detail in Ref. [1], here we provide the actual numerical values of all parameters. The force field

TABLE II. Parameters of the bonded interaction of the force field. The first and second columns contain the coefficients of terms diagonal in the internal coordinates of the chains, while the third and fourth ones contain the coefficients of the off-diagonal terms.

r_0^{CC} [Å]	1.53	$k_{r,\theta}^{HCH}$ [kcal/(mol Å)]	0
k^{CC} [kcal/(mol Å²)]	617.058	$k_{r1,r2}^{HCH}$ [kcal/(mol AA²)]	0
r_0^{CH} [Å]	1.09	$k_{r1,\theta}^{CCH}$ [kcal/(mol Å)]	-34.0818
k^{CH} [kcal/(mol Å²)]	654.455	$k_{r2,\theta}^{CCH}$ [kcal/(mol Å)]	0
k^{HCH} [kcal/mol]	76.952	$k_{r1,r2}^{CCH}$ [kcal/(mol Å²)]	0
θ_0^{HCH} [°]	107.899	$k_{r,\theta}^{CCC}$ [kcal/(mol Å)]	-54.494
k^{CCH} [kcal/mol]	85.726	$k_{r1,r2}^{CCC}$ [kcal/(mol Å²)]	25.9337
θ_0^{CCH} [°]	109.469	$G^{CC:CH}$ [kcal/mol]	-6.0034
k^{CCC} [kcal/mol]	107.446	$G^{CC:HH}$ [kcal/mol]	-3.6409
θ_0^{CCC} [°]	110.999	$G^{CH:CC}$ [kcal/mol]	2.9127
V^{HCCH} [kcal/mol]	0.2776	$G^{CH:CH}$ [kcal/mol]	0
V^{CCCH} [kcal/mol]	0.2776	$F^{H:CC:H}$ [kcal/mol]	-16.0398
V^{CCCC} [kcal/mol]	0.2776	$F^{C:CC:H}$ [kcal/mol]	-15.5343
		$F^{C:CC:C}$ [kcal/mol]	-33.3664

consists of bonded and nonbonded interactions. The bonded interactions involve bond stretching, angle bending, and torsions, as well as off-diagonal, or cross terms, coupling together the different internal coordinates of the chains. The corresponding terms have the form of the following expressions:

(a) Bond stretching, applying to all C-C and C-H bonds:

$$U(r) = \frac{1}{2} k^{IJ}(r-r_0)^2. \qquad (A1)$$

(b) Angle bending, applying to all C-C-C, C-C-H, and H-C-H angles:

$$U(\theta) = \frac{1}{2} k^{IJK}(\cos\theta - \cos\theta_0)^2. \qquad (A2)$$

(c) Torsion terms, applying to all C-C-C-C, C-C-C-H, and H-C-C-H sequences,

$$U(\varphi) = \frac{1}{2} V^{IJKL}(1 + \cos 3\varphi), \qquad (A3)$$

where φ is the torsional angle ($\varphi = 0$ corresponds to cis and $\varphi = \pi$ corresponds to trans). Throughout the rest of the paper, we use also torsional angle ϕ defined as a fluctuation of φ from the trans value, $\phi = \varphi - \pi$.

(d) Bond-angle and bond-bond cross terms, applying to all C-C-C, C-C-H, and H-C-H angles,

$$U(r_1, r_2, \theta) = k_{r_1,\theta}^{IJK}(r_1 - r_{10})(\cos\theta - \cos\theta_0) + k_{r_2,\theta}^{IJK}(r_2 - r_{20})$$
$$\times (\cos\theta - \cos\theta_0) + k_{r_1,r_2}^{IJK}(r_1 - r_{10})(r_2 - r_{20}), \qquad (A4)$$

where r_1 and r_2 are the bond lengths of the I-J and J-K bonds adjacent to an IJK bond angle θ.

(e) One-center angle-angle cross terms, applying to all pairs of bond angles about a tetrahedral carbon atom sharing a common bond,

$$U(\theta_1, \theta_2) = G^{IJ:KL}(\cos\theta_1 - \cos\theta_t)(\cos\theta_2 - \cos\theta_t), \qquad (A5)$$

where θ_1, θ_2 are the JIK and JIL bond angles, respectively, and I is the tetrahedral carbon. Here, θ_t is the tetrahedral angle.

(f) Two-center angle-angle cross terms, applying to all C-C-C-C, C-C-C-H, and H-C-C-H sequences,

$$U(\varphi, \theta_1, \theta_2) = F^{I:JK:L}\cos\varphi(\cos\theta_1 - \cos\theta_t)(\cos\theta_2 - \cos\theta_t), \qquad (A6)$$

where φ is the torsional angle corresponding to the sequence $IJKL$, θ_1, θ_2 are the IJK and JKL bond angles and θ_t is again the tetrahedral angle. Numerical values of all the parameters in the above expressions are contained in Table II.

The nonbonded interaction has the form $U(r) = Ae^{-Br} - Cr^{-6}$ between atoms on different chains and atoms on the same chain separated by more than two bonds (1–2 and 1–3 interactions are excluded). Numerical values of all the parameters for all three pairs of atoms (C-C, H-H, and C-H) are contained in Table III. Details concerning cutoff and long-range corrections can be found in Ref. [1].

TABLE III. Parameters of the nonbonded interaction of the force field.

Atoms	A [kcal/mol]	B [Å^{-1}]	C [Å^6 kcal/mol]
C-C	14889.0	3.089	639.58
H-H	2640.2	3.739	27.39
C-H	4300.9	3.416	137.44

APPENDIX B

In this appendix we discuss in detail the origin of the quantitative discrepancy between the slope of the c versus $\frac{1}{2}\langle(\phi_0-\phi_1)^2\rangle$ line as obtained from formula (5) and from our quantum simulation data (Fig. 10). To this end, we have to look more closely at the way the formula has been derived in Ref. [3]. The model used assumes a single chain consisting of rigid C-C bonds with length a and rigid C-C-C angles $\theta_{CCC}=\pi-\alpha$, subject to torsional deformations only. The expression (5) then evaluates c simply as the average end-to-end distance between carbon atoms separated by four bonds. Let us denote by $\vec{r},\vec{r}'$ the instantaneous positions of the two atoms, and by $\vec{r}_0,\vec{r}_0'$ their equilibrium positions around which they oscillate with instantaneous fluctuations $\vec{\Delta},\vec{\Delta}'$. The squared end-to-end distance is then given by

$$(\vec{r}-\vec{r}')^2=(\vec{r}_0-\vec{r}_0'+\vec{\Delta}-\vec{\Delta}')^2=(\vec{r}_0-\vec{r}_0')^2+(\vec{\Delta}-\vec{\Delta}')^2,$$
(B1)

where the cross term has vanished, because the fluctuations $\vec{\Delta},\vec{\Delta}'$ are orthogonal to $\vec{r}_0-\vec{r}_0'$ (since the bond lengths and angles are assumed to be rigid, the only possible small displacements of carbon atoms are those perpendicular to the plane of the unperturbed all-trans chain). This expression contains, apart from the squared distance between the equilibrium positions $(\vec{r}_0-\vec{r}_0')^2$, which is directly related to the lattice constant c, also a fluctuation term. Neglecting this term for a relatively short segment of chain, as done in Ref. [3], results in underestimating of the thermal contraction. In order to improve on this, one has to consider a longer segment of the chain, which would, however, require a knowledge of correlation functions between torsions displaced by more than one bond. This is clearly impossible within the simple single-chain model assumed in Ref. [3], where the crystal environment of the chain is neglected entirely. This together with a separable torsional potential classically leads to vanishing of all correlation functions between displaced torsions, and in turn to coiling of longer segments of a chain. In a crystal it is just the external nonbonded field of all other chains acting directly on the absolute coordinates of the atoms of a given chain (rather than on the torsional angles, which by their very nature have a character of relative coordinates), which induces nonzero correlations between the torsions in the chain. These correlations reflect the existence of the underlying 3D crystal structure with its translational long-range order and result in an overall coherent shortening of the chain, instead of its coiling. The quantitative agreement of the formula with experiment, as stated in Ref. [3], thus appears to be accidental and arises due to compensation of two effects: neglecting the crystal field contribution lowers the effective torsional constant by a factor of two, which in turn increases the torsional fluctuations and compensates for the lower value of the proportionality constant in expression (5).

Now we derive a few formulas similar to Eq. (5), taking into account progressively longer segments of a chain. In general, we are interested in calculating the end-to-end distance of a segment of a chain consisting of $n=2m$ bonds. The corresponding vector can be expressed as [21]

$$\vec{R}_n=\sum_{k=1}^{n}\prod_{i=0}^{k-1}T_i(a,0,0)^T,$$
(B2)

where the 3×3 matrices T_i are defined as follows:

$$T_i=\begin{vmatrix} \cos\alpha & \sin\alpha & 0 \\ \sin\alpha\cos\phi_i & -\cos\alpha\cos\phi_i & \sin\phi_i \\ \sin\alpha\sin\phi_i & -\cos\alpha\sin\phi_i & -\cos\phi_i \end{vmatrix},$$
(B3)

angles ϕ_i being the torsional angles. Evaluating $\langle|\vec{R}_n|\rangle$ and keeping just terms up to second order in the angles ϕ_i we find the following approximations $c^{(m)}=(1/m)\langle|\vec{R}_{2m}|\rangle$ to the contracted lattice constant c (the actual calculation has been performed by MATHEMATICA):

$$c^{(2)}=\frac{1}{2}\langle|\vec{R}_4|\rangle=c_0\left[1-\frac{1}{4}\sin^2\frac{\alpha}{2}(\langle\phi_0^2\rangle-\langle\phi_0\phi_1\rangle)\right],$$

$$c^{(3)}=\frac{1}{3}\langle|\vec{R}_6|\rangle=c_0\left[1-\frac{1}{9}\sin^2\frac{\alpha}{2}(4\langle\phi_0^2\rangle-5\langle\phi_0\phi_1\rangle+2\langle\phi_0\phi_2\rangle-\langle\phi_0\phi_3\rangle)\right],$$

$$c^{(4)}=\frac{1}{4}\langle|\vec{R}_8|\rangle=c_0\left[1-\frac{1}{16}\sin^2\frac{\alpha}{2}(10\langle\phi_0^2\rangle-14\langle\phi_0\phi_1\rangle+8\langle\phi_0\phi_2\rangle-5\langle\phi_0\phi_3\rangle+2\langle\phi_0\phi_4\rangle-\langle\phi_0\phi_5\rangle)\right],$$
(B4)

$$c^{(5)} = \frac{1}{5}\langle|\vec{R}_{10}|\rangle = c_0\Bigg[1 - \frac{1}{25}\sin^2\frac{\alpha}{2}(20\langle\phi_0{}^2\rangle - 30\langle\phi_0\phi_1\rangle + 20\langle\phi_0\phi_2\rangle - 14\langle\phi_0\phi_3\rangle$$

$$+ 8\langle\phi_0\phi_4\rangle - 5\langle\phi_0\phi_5\rangle + 2\langle\phi_0\phi_6\rangle - \langle\phi_0\phi_7\rangle)\Bigg],$$

$$c^{(6)} = \frac{1}{6}\langle|\vec{R}_{12}|\rangle = c_0\Bigg[1 - \frac{1}{36}\sin^2\frac{\alpha}{2}(35\langle\phi_0{}^2\rangle - 55\langle\phi_0\phi_1\rangle + 40\langle\phi_0\phi_2\rangle - 30\langle\phi_0\phi_3\rangle + 20\langle\phi_0\phi_4\rangle - 14\langle\phi_0\phi_5\rangle + 8\langle\phi_0\phi_6\rangle$$

$$- 5\langle\phi_0\phi_7\rangle + 2\langle\phi_0\phi_8\rangle - \langle\phi_0\phi_9\rangle)\Bigg],$$

where $c_0 = 2a\cos(\alpha/2)$ is the lattice constant of the unperturbed chain.

We introduce now off-plane displacements z_i of carbon atoms along local z axes defined for each C atom by the unit vector $\vec{k}_i = (\vec{a}_i \times \vec{a}_{i+1})/a^2\sin\alpha$, where $\vec{a}_i$ is the vector connecting carbon atoms $i-1$ and i. Vectors $\vec{k}_i$ are perpendicular to the plane of the all-trans chain and their directions alternate below and above the plane. It can then be easily shown [4] that the torsional angles ϕ_i defined via $\cos\phi_i = -(\vec{a}_{i-1} \times \vec{a}_i)\cdot(\vec{a}_i \times \vec{a}_{i+1})/a^4\sin^2\alpha$, or, alternatively, $\sin\phi_i = \vec{a}_{i-1}\cdot(\vec{a}_i \times \vec{a}_{i+1})/a^3\sin^2\alpha$, can be in first order in displacements z_i expressed as $\phi_i = (-z_{i-2} - z_{i-1} + z_i + z_{i+1})/a\sin\alpha$. Upon substitution of this latter expression to Eq. (B4), we find

$$c^{(m)} = c^{(\infty)} + \frac{1}{2m^2}\frac{\langle(z_0 - z_{2m})^2\rangle}{c_0}, \quad \text{(B5)}$$

where

$$c^{(\infty)} = c_0\left(1 - \frac{\langle(z_0 - z_2)^2\rangle}{2c_0^2}\right) \quad \text{(B6)}$$

is the limiting $m \to \infty$ value of the contracted lattice constant c. The last result has been derived also in Ref. [4] by means of a simple geometrical argument, expressing c as a projection of the segment consisting of two C-C bonds, whose end-to-end length is c_0, on the plane of the unperturbed chain.

Applying the formula for $c^{(3)}$ corresponding to a segment consisting of six C-C bonds to our simulation data, we find a slope that is still larger by about 50% than the theoretical one. A characteristic property of all the expressions (B4) is that the coefficients of torsion correlation functions increase in magnitude with the length of the segment. The correct limiting result for thermal contraction thus emerges progressively as a consequence of a delicate cancellation between the terms, which means that a knowledge of correlation functions at many different displacements with very good accuracy would be required. Such behavior reflects the lack of existence of a preferred crystal direction for a chain in the formulation employing exclusively torsional angles. In contrast to this, upon substitution of the true off-plane displacements of the atoms into these expressions, the limiting exact result emerges in a very simple form, which has a clear geometrical interpretation and contains just a single correlation function between second neighbors. This demonstrates that while the relation between the torsional fluctuations and the lattice constant c provides a very useful insight for qualitative understanding of the thermal contraction of c, it would be at the same time hard to push these considerations to a truly quantitative level.

[1] R. Martoňák, W. Paul, and K. Binder, J. Chem. Phys. **106**, 8918 (1997).

[2] D. J. Lacks and G. C. Rutledge, J. Phys. Chem. **98**, 1222 (1994).

[3] R. A. Stobbe and P. C. Hägele, J. Polym. Sci., Part B, Polym. Phys. **34**, 975 (1996).

[4] R. A. Stobbe, Ph.D. Thesis, Universität Ulm, Abteilung Angewandte Physik, 1996 (unpublished).

[5] T. A. Scott, Phys. Rep. **27**, 89 (1976).

[6] K. A. Müller and H. Burkard, Phys. Rev. B **19**, 3593 (1979).

[7] D. M. Ceperley and E. L. Pollock, in *Monte Carlo Method in Theoretical Physics*, edited by S. Caracciolo and A. Fabrocini (ETS, Pisa, 1991).

[8] M. H. Müser, P. Nielaba, and K. Binder, Phys. Rev. B **51**, 2723 (1995).

[9] C. Rickwardt (private communication).

[10] R. Martoňák, W. Paul, and K. Binder, Comput. Phys. Commun. **99**, 2 (1996).

[11] R. Martoňák, W. Paul, and K. Binder, J. Comp. Aid. Mat. Des. **4**, 9 (1997).

[12] R. A. Sorensen, W. B. Liau, L. Kesner, and R. H. Boyd, Macromolecules **21**, 200 (1988).

[13] M. F. Herman, E. J. Bruskin, and B. J. Berne, J. Chem. Phys. **74**, 4078 (1981).

[14] *Quantum Monte Carlo Methods in Equilibrium and Nonequilibrium Systems*, Proceedings of the Ninth Taniguchi International Symposium, Susono, Japan, 1986, edited by M. Suzuki

(Springer-Verlag, Berlin, 1987).

[15] N. Karasawa, S. Dasgupta, and W. A. Goddard III, J. Phys.Chem. **95**, 2260 (1991).

[16] M. P. Allen and D. J. Tildesley, *Computer Simulation of Liquids* (Clarendon Press, Oxford, 1990).

[17] G. Dadobaev and A. I. Slutsker, Fiz. Tverd. Tela (Leningrad) **23**, 1936 (1981) [Sov. Phys. Solid State **23**, 1131 (1981)].

[18] M. Parrinello and A. Rahman, J. Chem. Phys. **76**, 2662 (1982).

[19] A. A. Gusev, M. M. Zehnder, and U. W. Suter, Phys. Rev. B **54**, 1 (1996).

[20] G. C. Rutledge, D. J. Lacks, R.f Martoňâk, and K. Binder (unpublished).

[21] P. J. Flory, *Statistical Mechanics of Chain Molecules* (Hanser Publishers, Munich, 1989).